NANOSYSTEMS: PHYSICS, CHEMISTRY, MATHEMATICS, 2013, 4 (2), P. 269–275

PHOTOLUMINESCENCE IN Fe^{3+} ION DOPED BARIUM TITANATE NANOPARTICLES

P. Barik[1], T. K. Kundu[1]

[1] Department of Physics, Visva-Bharati University, Santiniketan-731235, W.B., India

pbarik_mid1983@yahoo.co.in, tapaskumar.kundu@visva-bharati.ac.in

PACS 78.67.Bf, 78.55.Qr

Fe^{3+} ion doped barium titanate (BT) nanopowders were synthesized by the sol gel route. The average size of tetragonal bariun titanate (t-BT) powders lies in the range 16–40 nm. The specimens show ultraviolet (UV) emission (peak at 376 nm) along with emission in violet, blue, green and yellow color. The blue band (peak at 452 nm) is seen to grow significantly with annealing temperature. This band arises due to Ti^{3+} defects which are stabilized by Fe^{3+} ions in BT specimens. The samples show two distinct Electron Paramagnetic Resonance (EPR) bands of g-value around 4.11 and 1.98, which originated from Fe^{3+} ions and Ti^{3+} defects respectively. A correlation between the photoluminescence (PL) and EPR band intensity, grown from same species, was found.

Keywords: barium titanate, photoluminescence, nanoparticles.

1. Introduction

Pure Barium Titanate ($BaTiO_3$, BT) and transition metal ion-doped BT have important applications in electromechanical devices such as capacitors, transducers, thermistors, actuators, humidity sensors etc [1-4]. BT also has interesting optical properties with potential application in high-density optical data storage, laser power combining and optical computing [5]. Of all the known defects in BT, iron is easily soluble and has a significant effect on the optical properties of BT [6-8]. Katyar et al observed a structure-less visible emission band in BT at 500 nm at low temperature revealing lower emission energy than its band gap [9]. BT nanocrystals (nc-BT) show relatively enhanced photoluminescence (PL) emission [9, 10]. Various reports were published to describe the origin of the visible emission shown by BT [11-13]. It was reported that the emission is related to the charge transfer between titanium and oxygen atoms. The luminescence from bulk BT was ascribed to the presence of self-trapped excitons (STE) within TiO_6 octahedra, viz $Ti^{3+} - O^-$ STE [10]. Zhang et al established that the PL of BT is due to localized states promoted by the intrinsic defect distribution (oxygen vacancy) [14]. Those states essentially decrease the band gap energy of BT. Recently, a group has established that both five-fold and six-fold oxygen-Ti coordination exist in amorphous BT systems, which is responsible for PL in disorder materials [15-17]. Therefore, from the above discussions it seems that more investigations are required in this field to understand the origin of the emission shown by BT.

PL emission from an acceptor doped or Fe-doped BT system are of particular interest in this work. Here, we report the emission from Fe^{3+}-doped nc-BT powders. The emission appears both in ultraviolet and visible range of wavelength. PL emissions have correlation with electron paramagnetic resonance (EPR) signals shown by the specimens.

2. Experimental

Iron ion doped BT ultrafine powder were synthesized by the sol-gel hydroxide method using barium hydroxide [$Ba(OH)_2{\cdot}8H_2O$, Merck], tetraisopropyl orthotitanate [$Ti(C_3H_7O)_4$, Merck] and iron(III) nitrate [$Fe(NO_3)_3{\cdot}9H_2O$, Merck] as starting materials [18]. Here, the powders were doped with 2 mole% of Fe^{3+}. The concentration of the dopant was chosen within the solubility limit of Fe^{3+} in BT [19]. $Ba(OH)_2{\cdot}8H_2O$ was dissolved in ethanol and glacial acetic acid (1:1 volume ratio) by stirring and heating the solution at 50-70 °C. After cooling the solution to room temperature a stoichiometric amount of tetraisopropyl orthotitanate was added drop wise. Then, a calculated amount of iron nitrate, prepared separately, was added to the above solution. The clear solution, which was obtained after stirring for a few minutes, was allowed to gel at room temperature. The dried gel-powders were calcined at different temperatures between 400-700 °C for two hours in a tube furnace to obtain doped nc-BT powders. XRD patterns of the specimens were recorded using Phillips powder Diffractometer. The microstructures of the samples were investigated by a TEM of JEOL. A Perkin-Elmer luminescence spectrometer was used to study the light emission from the samples. The EPR spectra were recorded at an X-band frequency (∼9.43 GHz) with a Varian Associates spectrometer.

3. Results and discussions

Figure 1 shows X-ray diffraction patterns of 2 mole % iron ion doped BT powders obtained by heating the gel-powders at different temperatures. We have calculated interplanar spacing (d_{hkl}) values, corresponding to each of the diffraction peaks. Specimen 'a', gel-powders annealed at 400 °C, shows a set of d_{hkl} values that matches with an orthorhombic (o-BT-II) crystal structure (P_{nma} space group), with average lattice parameters a=0.6435 nm, b=0.5306 nm, and c=0.8854 nm. The observed d_{hkl} values are reproduced with a standard deviation of ±0.0005 nm. The orthorhombic phase (o-BT-II) is structurally different from conventional orthorhombic BT. A thorough analysis by the Rietveld method was given in our previous reports [19, 20]. Specimens 'b' and 'c', heating the gel-powders at 600 °C and 700 °C respectively, contain two sets of d_{hkl} values. One set is due to standard tetragonal BT phase and other set of d_{hkl} values arise due to orthorhombic crystal structure. A large fraction of the o-BT-II is promoted to t-BT at a temperature of 700 °C via a surface diffusion limited o→t transformation process. The average diameter (D) of the grains was determined from the FWHM values in the XRD peaks by using Debye-Scherrer relation $d_{XRD} = k\lambda/\beta(\theta)\cos(\theta)$, where λ is the wavelength of X-ray, β the FWHM of the (200) peak, θ the diffraction angle and the constant $k \approx 1$. The average sizes of 16 nm and 40 nm were obtained for the t-BT samples annealed at 600 °C and 700 °C respectively.

The grain size of the nanocrystalline ceramics was also estimated using transmission electron microscope (TEM). A typical micrograph from specimen 'c' is shown in Fig. 2a. The corresponding diffraction patterns are shown in Fig. 2b. There is a distribution of particle sizes in the specimens. The results estimated from TEM reasonably agree with those obtained from XRD.

Figure 3 shows EPR spectra of the specimens after heating the powders at (a) 400 °C, (b) 600 °C, and (c) 700 °C for 2 h in air. The samples show two distinct EPR bands (Band I and Band II) of g-value around 4.11 and 1.98. The intensity of Band-II increases by 55% as the sintering temperature rises from 400 °C to 700 °C. The positions of the signals are not altered significantly. The reverse trend is observed for the Band I

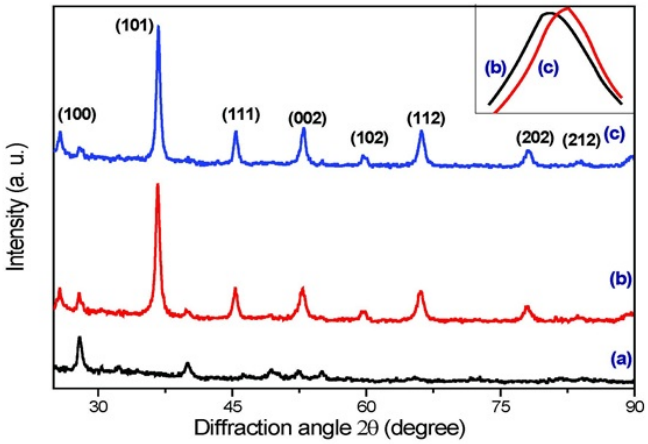

Fig. 1. XRD patterns for 2% Fe-doped BT nanopowders after heating a sol-gel precursor at (a) 400 ° C and (b) 600 ° C (c) 700 ° C for 2 hr in air. A close-up in the inset compares the shift in (101) peak of sample (b) and (c)

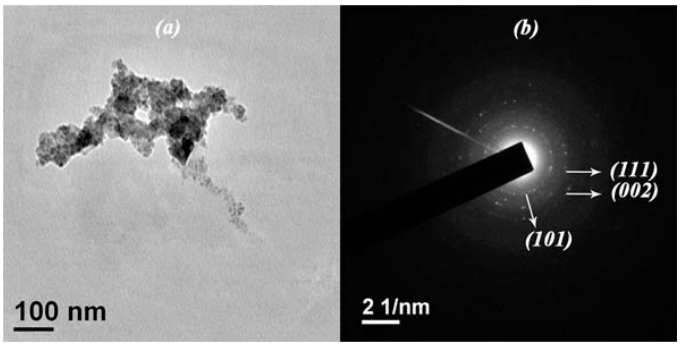

Fig. 2. A typical (a) TEM image and (b) Diffraction pattern taken from specimen 'c' heat-treated at 700 ° C for 2hr. The diffraction rings in the pattern (from center to edge) can be indexed as the (101), (111), and (002) peaks of a tetragonal (P_{4mm}) BT phase

signal, as its intensity is decreased by 58% with the same change in sintering temperature. Thus, when the Band I signal is strong, the Band II signal is weak and vise versa. The O_i^- is a common EPR sensitive species ($g \sim 2$) in oxides [21, 22]. A peak at g=1.97 was reported in BT due to localized Ti^{3+} states [23]. In the present case, intensity of the signal at g = 1.98 have increased with the annealing temperature and the doped specimens show an extra EPR peak (g = 4.11). EPR studies of Fe^{3+} ($3d^5$, $S = 5/2$) in the tetragonal phase have been reported previously [24-26]. In a large number of Fe^{3+}-containing materials, a symmetric and isotropic line at $g \approx$4.0–4.2 as well as a line at $g = 2.0$ was observed. In our case, the g-value at 4.11 indicates that the iron ions are trivalent and the site symmetry is slightly distorted octahedral. Here, the Fe^{3+} occupies the Ti^{4+} sites which produce distorted octahedral symmetry. This case produces a low symmetry site structure. As the Fe^{3+} ions occupy the Ti^{4+} sites, EPR response of Fe^{3+} doped BT may be expected to exhibit changes upon crystallization due to removal of distortion around various ions in the BT. This argument is supported by our experimental observation where the signal intensity of Band I decreases with annealing temperature. Band II that grows with annealing temperature can originate either due to species Fe^{3+} or Ti^{3+}. In the absence of Fe^{3+} ions,

the same signal is eliminated with increased annealing temperatures. The appearance of a few emission bands from the doped BT specimens, when excited properly, corroborates the EPR results.

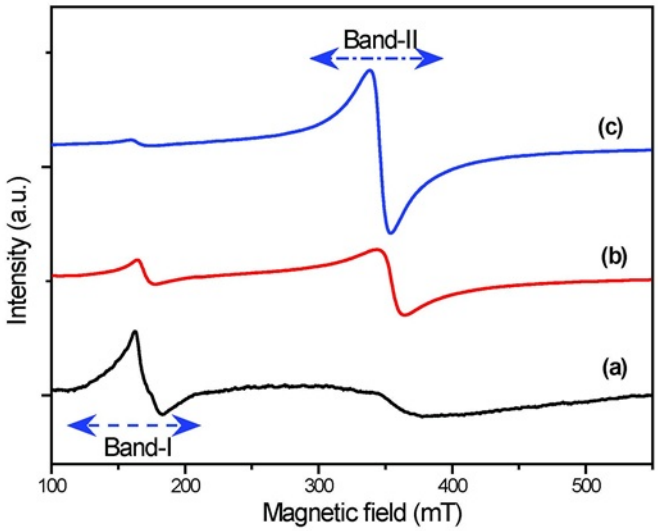

Fig. 3. EPR spectra for 2% Fe doped BT nanopowders after heating a sol-gel precursor at (a) 400 ° C, (b) 600 ° C, and (c) 700 ° C for 2 hr in air

The emission spectra from the specimens, irradiated at 250 nm by a xenon lamp, are shown in Fig. 4. The excitation energy was chosen from the excitation spectra of the specimens which show an intense peak at 250 nm. The spectra are analyzed by fitting with multiple Gaussian curves. A typical Gaussian fitting of PL spectrum from the specimen '*c*' is shown in Fig. 5. The composite specimens, '*b*' and '*c*', also show same bands with different intensity level and shifted peak positions. The UV emission peak shifts significantly to higher wavelengths with increasing annealing temperatures. Typically the peak at 376 nm in specimen '*a*' is shifted to 395 nm in specimen '*c*'. It is evident from Gaussian fitting data that the band intensity of 421 nm and 619 nm line decreases and other bands grow on annealing the powder at temperature as high as 600 ° C or above. Among the bands, the growth of 452 nm line is distinct and significant.

The band gap of BT lies between 3–3.2 eV, as obtained from optical absorption edges [27]. Thus, the energy corresponding to the 250 nm line makes a direct transition and the UV emission band is assigned to a direct band gap transition. The band gap energy of nc-BT has increased to 4.9 eV according to the excitation maxima. Luminescence at ~2.96 eV (421–424 nm) is caused by the transition from the near conduction band edge to the valance band. It is argued that the electronic band structure of BT has a low-lying narrow conduction bands resulting from defects [28]. In amorphous materials, nonbridging oxygens (i.e. ones which are bonded to a single main group atom) participate in ionic interactions to form a typical network like Ti-O. Crystallization into a single o- or t-BT polymorph can lead to the elimination of defects or imperfections, particularly of nonbridging oxygen of a TiO_5 group, in which Ti is penta-coordinated by oxygen. A decrease in the intensity of the 421 nm line, as observed experimentally, supports these statements. The recombination process corresponding to the charge transfer from the central Ti^{3+} to adjacent V_0^+ states in the TiO_5 groups leads to a luminescence peak centered at 452 nm.

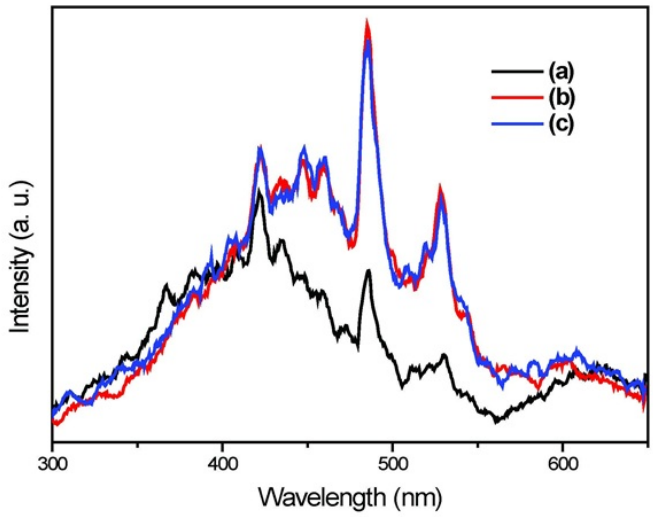

Fig. 4. Photoluminescence spectra for 2% Fe doped BT nanopowders after heating a sol-gel precursor at (a) 400 ° C, (b) 600 ° C, and (c) 700 ° C for 2 hr in air

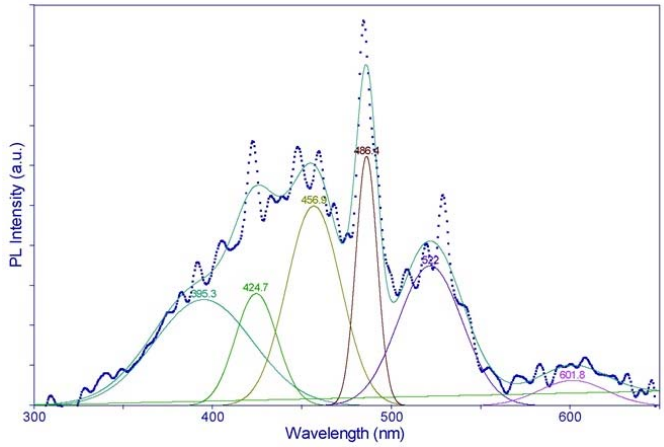

Fig. 5. Photoluminescence emission spectra of the specimen heated at 700 ° C for 2 hr fitted with Gaussian curves

The energy interval (~2.75 eV) between $Ti^{3+}(3d^1)$- and V_0^+ states supports the emission at a wavelength of 452 nm. Experimentally, the band is observed to grow considerably with annealing at higher temperatures. If it is considered that EPR Band II originates from Ti^{3+} species then a correlation between the PL band and EPR band intensity is found. The intensities of both signals increase with higher annealing temperatures. In that case, Fe^{3+} ions certainly play an important role in stabilizing Ti^{3+} defects in BT, even samples sintered at higher temperatures. In amorphous and composite materials, a large amount of "broken" surfaces or dangling bonds and color centers intrinsically exist either in a distorted structure or a highly strained lattice (as in this example of o-/t-BT-nanocrystals) and involve a series of E_{em} levels localized within the forbidden gap. They very sensitively tailor the light emission in multiple bands at room temperature. The blue emission at 485 nm (~2.57 eV) is attributed to the intraband transitions from self-trapped excitons [28, 29]. It is also evident from Gaussian fitting data that a prominent yellow emission is centered at ~2.38 eV (520–524 nm) and its intensity increases as the sintering

temperature increases. The electrons' polarons interact with holes, possibly trapped near crystal defects or impurities, and form an intermediate state: self-trapped exciton (STE). These self-trapped excitons contributed to the 485 nm and 520 nm emissions [10, 30]. The band at 620–600 nm is explained in terms of the transition from Fe^{3+} states to the valence band of BT. The intensity of this band decreases with annealing temperature and a correlation with EPR band I grown from the same species is found. The existence of Fe^{3+} energy states in BT was earlier established from optical absorption data [8]. PL measurements and optical absorption studies of nc-BT powders that are heat-treated under different atmospheres would provide much useful information.

4. Conclusions

BT nanopowders doped with 2 mole % Fe^{3+} ions were synthesized by the sol gel route. The gel-powders annealed at 400 °C show orthorhombic BT (*o*-BT-II) crystal structure. The *o*-BT-II phase begins to transform to t-BT on heating the specimens at temperatures as high as 600 °C. The average size of t-BT powders range from 16–40 nm. The samples show two distinct EPR bands (Band I and Band II) of *g*-value around 4.11 and 1.98. The Band I signal (g=4.11) originates due to isolated Fe^{3+} ions in low symmetry site at low temperatures. As the Fe^{3+} ions occupy the Ti^{4+} sites, the EPR response exhibits changes upon crystallization due to removal of distortion around various ions in the BT. Band II, which grows with annealing temperature, originates due to Ti^{3+} defects stabilized by Fe^{3+}. The specimens show UV emission (peak at 376 nm) along with the emission in violet, blue, green and yellow color (421, 452, 485, 526, 619 nm). The redshift of the UV emission band is primarily caused by quantum size effects. The blue band (452 nm) is seen to grow with annealing temperatures due to Ti^{3+} defects which are stabilized by Fe^{3+} in the doped specimens. A correlation between the PL band and EPR band intensity, grown from same species, was found.

Acknowledgement

The work was supported by the grant from the Nano Science and Technology Initiative of the Department of Science and Technology, and University Grant Commission, New Delhi.

References

[1] Sahoo T., Tripathy S.K., et al. Microstructural and photo luminescence studies on hydrothermally synthesized Ce-doped barium titanate nanocrystals. *Materials Science and Engineering: B.*, **131**(1-3), P. 277–280 (2006).

[2] Yu J., Sun J., et al. Light-emission properties in nanocrystalline $BaTiO_3$. *Applied Physics Letters.*, **77**(18), P. 2807–2809 (2000).

[3] Pizani P.S., Basso H.C., et al. Visible photoluminescence in amorphous ABO_3 perovskites. *Applied Physics Letters*, **81**(2), P. 253–255 (2002).

[4] Pizani P.S., Leite E.R., et al. Photoluminescence of disordered ABO_3 perovskites. *Applied Physics Letters*, **77**(6), P. 824–826 (2000).

[5] Gunter P., Huignard J.P., *Photorefractive materials and Their Application I and II. Topic in Applied Physics*, Vol. 61 and 62. Springer-Verlag, Berlin, (1988 and 1989).

[6] Klein M.B., Schwartz R.N., Photorefractive effect in $BaTiO_3$: microscopic origins. *Journal of the Optical Society of America B: Optical Physics*, **3**(2), P. 293–305 (1986).

[7] Schunemann P.G., Temple D.A., et al. Role of iron centers in the photorefractive effect in barium titanate. *Journal of the Optical Society of America B: Optical Physics*, **5**(8), P. 1685–1696 (1988).

[8] Mazur A., Schirmer O.F., et al. Optical absorption and light-induced charge transport of Fe^{2+} in $BaTiO_3$. *Applied Physics Letters*, **70**(18), P. 2395–2397 (1997).

[9] Katiyar R.S., Meng J.F., et al. Effect of grain size and Pb dopant on luminescence in $BaTiO_3$. *Journal of Vacuum Science & Technology A*. **15**(6), P. 2945–2948 (1997).
[10] Meng J., Huang Y., et al. Photoluminescence in nanocrystalline $BaTiO_3$ and $SrTiO_3$. *Physics Letters A*, **205**(1), P. 72–76 (1995).
[11] Dey S.K., Leeg R.Z., Processing and parameters of sol-gel PZT thin-films for GaAs memory applications. *Ferroelectrics*, **112**(1), P. 309–319 (1990).
[12] Leonelli R., Brebner J.L., Time-resolved spectroscopy of the visible emission band in strontium titanate. *Physical Review B*, **33**(12), P. 8649–8656 (1986).
[13] Bouma B., Blasse G., Dependence of luminescence of titanates on their crystal structure. *Journal of Physics and Chemistry of Solids*, **56**(2), P. 261–265 (1995).
[14] Zhang M.S., Yin Z., et al. Study of structural and photoluminescent properties in barium titanate nanocrystals synthesized by hydrothermal process. *Solid State Communications*, **119**(12), P. 659–663 (2001).
[15] Souza I.A., Gurgel M.F.C., et al. Theoretical and experimental study of disordered $Ba_{0.45}Sr_{0.5}5TiO_3$ photoluminescence at room temperature. *Chemical Physics*, **322**(3), P. 343–348 (2006).
[16] Orhan E., Varela J.A., et al. Room-temperature photoluminescence of $BaTiO_3$: Joint experimental and theoretical study. *Physical Review B*, **71**(8), P. 085113–085119 (2005).
[17] Silva M.S., Cilense M., et al. The nature of the photoluminescence in amorphized PZT. *Journal of Luminescence*, **111**(3), P. 205–213 (2005).
[18] Beck H.P., Eiser W., et al. Pitfalls in the synthesis of nanoscaled perovskite type compounds. Part I: Influence of different so-gel preparation methods and characterization of nanoscaled $BaTiO_3$. *Journal of the European Ceramic Society*, **21**(6), P. 687–693 (2001).
[19] Jana A., Kundu T.K., et al. Dielectric behavior of Fe-ion-doped $BaTiO_3$ nanoparticles. *Journal of Applied Physics*, **97**(4), P. 044311–044316 (2005).
[20] Jana A., Ram S., et al. $BaTiO_3$ nanoparticles of orthorhombic structure following a polymer precursor. Part I. X-ray diffraction and electron paramagnetic resonance. *Philosophical Magazine B*, **87**(35), P. 5485–5495 (2007).
[21] Hoffmann K., Hahn D., Electron Spin Resonance of Lattice Defects in Zinc Oxide. *Physica status solidi (a)*, **24**(2), P. 637–648 (1974).
[22] Ram S., Kundu T.K., Synthesis and Unusual Electron Paramagnetic Resonance Spectrum of Metastable Nanoclusters of ZnO Semiconductor Crystallites. *Journal of Nanoscience and Nanotechnology*, **4**(8), P. 1076–1080 (2004).
[23] Kutty T.R.N., Murugaraj P., EPR study on the role of Mn in enhancing PTC of $BaTiO_3$. *Materials Letters*, **3**(5-6), P. 195–199 (1985).
[24] Hornig A.W., Rempel R.C., et al. Interpretation of Electron Paramagnetic Resonance in $BaTiO_3$. *Physical Review Letter*, **1**(8), P. 284–286 (1958).
[25] Kirkpatric E.S., Muller K.A., et al. Strong Axial Electron Paramagnetic Resonance Spectrum of Fe^{3+} in $SrTiO_3$ Due to Nearest-Neighbor Charge Compensation. *Physical Review*, **135**(1A), P. A86–A90 (1964).
[26] Maartense I., Magnetic Properties of Fe^{2+}-Doped $MnCO_3$. *Physical Review B*, **6**(11), P. 4324–4331 (1972).
[27] Cordona M., Optical Properties and Band Structure of $SrTiO_3$ and $BaTiO_3$. *Physical Review*, **140**(2A), P. A651–A655 (1965).
[28] Kim S.W., Fujita S., et al. Self-organized ZnO quantum dots on SiO_2/Si substrates by metalorganic chemical vapor deposition. *Applied Physics Letters*, **81**(26), P. 5036–5038 (2002).
[29] Brus L., Electronic wave functions in semiconductor clusters: experiment and theory. *The Journal of Physical Chemistry*, **90**(12), P. 2555–2560 (1986).
[30] Cho W.S., Hamada E., Planar defects and luminescence of $BaTiO_3$ particles synthesized by a polymerized complex method. *Journal of Alloys and Compounds*, **268**(1-2), P. 78–82 (1998).